ISSN 0965-5441, Petroleum Chemistry, 2018, Vol. 58, No. 4, pp. 317–329. © Pleiades Publishing, Ltd., 2018.
Published in Russian in Membrany i Membrannye Tekhnologii, 2018, Vol. 8, No. 2, pp. 116–128.

Study of Separation Behavior of Activated and Non-Activated MOF-5 as Filler on MOF-based Mixed-Matrix Membranes in H_2/CO_2 Separation[1]

Mehrzad Arjmandi[a], Majid Pakizeh[a, *], Mohammadreza Saghi[a], and Abolfazl Arjmandi[b]

[a] *Chemical Engineering Department, Faculty of Engineering, Ferdowsi University of Mashhad, Mashhad, Iran*
[b] *Department of Chemical Engineering, Mazandaran University of Science and Technology, Mazandaran, Iran*
**e-mail: pakizeh@um.ac.ir*

Received October 20, 2017

Abstract—In this study, cubic and tetragonal structures of MOF-5 (C-MOF-5 and T-MOF-5) were successfully synthesized, characterized and incorporated into cellulose acetate (CA) polymer matrix in the range of 6, 9 and 12 wt % to fabricate mixed matrix membranes (MMMs). The effects of smaller pore size of T-MOF-5 and more ZnO molecules in T-MOF-5, on the H_2 and CO_2 permeation properties of C-MOF-5/CA and T-MOF-5/CA MMMs were investigated. The all novel MMMs were prepared using the solution casting method and characterized by FTIR, TGA and SEM. SEM images as well as results of FTIR and TGA analyses confirmed good adhesion between both MOF-5s and CA matrix. Addition of both C-MOF-5 and T-MOF-5 into the CA improved the gas transport properties of the CA, especially in H_2 separation. The H_2/CO_2 selectivity continued the increasing trend at 9 wt % and did not significantly reduce even at 12 wt % due to good adhesion between both MOF-5s and CA. The highest H_2/CO_2 selectivity was obtained at 12 and 9 wt % loading of C-MOF-5 and T-MOF-5, respectively. By changing the filler from C-MOF-5 to T-MOF-5, the increasing and reducing of adsorption site of H_2 and CO_2 (respectively), and also reducing in pore size, caused the appearance of H_2 permeability to not change much but the CO_2 permeability to reduce. Accordingly, the H_2/CO_2 selectivity in all T-MOF-5/CA MMMs is higher than that in all C-MOF-5/CA MMMs. According to obtained results, the activated MOFs (i.e., C-MOF-5 in this study) are not always the best choices for separation process.

Keywords: mixed matrix membrane, metal organic framework, CA, C-MOF-5, T-MOF-5, gas separation
DOI: 10.1134/S0965544118040023

INTRODUCTION

Hydrogen has many applications in some areas such as hydrogenation of fuels, increasing the calorific value of gas streams, power fuel cell vehicles and generation of electrical energy. Currently, the majority of H_2 is produced by natural gas reforming (steam-methane reforming (SMR)). Before H_2 can be used, it should be purified of the resultant SMR gas mixture which basically contains CO_2 [1]. Also, highly pressurized pre-combustion streams have important advantages over post-combustion in Carbon capture and storage (CSS) with membranes. Accordingly, the H_2/CO_2 separation is very important in CSS [2, 3].

Therefore, a process to separation of H_2 from CO_2 is required [4]. Among various techniques, membrane separation processes have been widely used. The main advantages of membranes are their low capital cost and low energy requirements compared to those of other conventional separation techniques [5].

It is clear that research efforts must focus on improving the technologies for H_2/CO_2 separation. However, the fabrication of good H_2-permselective membranes is still a big challenge.

Several membrane technologies have been reported for H_2/CO_2 separation, including metallic [6–9], inorganic [10–12] and polymeric membranes [13, 14]. Polymeric membranes bring down the production costs and can be easily developed to hollow fiber modules or spiral wound. Permeability and selectivity are the two basic criteria of membranes and there is a trade-off limitation for polymeric membranes between these two parameters. The polymeric membranes have lower permeability and selectivity than inorganic membranes for gas separations [15, 16]. To improve polymeric membrane performance, considerable research has focused on the addition of various organic and inorganic nanomaterials such as carbon molecular sieves, zeolite, silica, titanium dioxide,

[1] The article is published in the original.

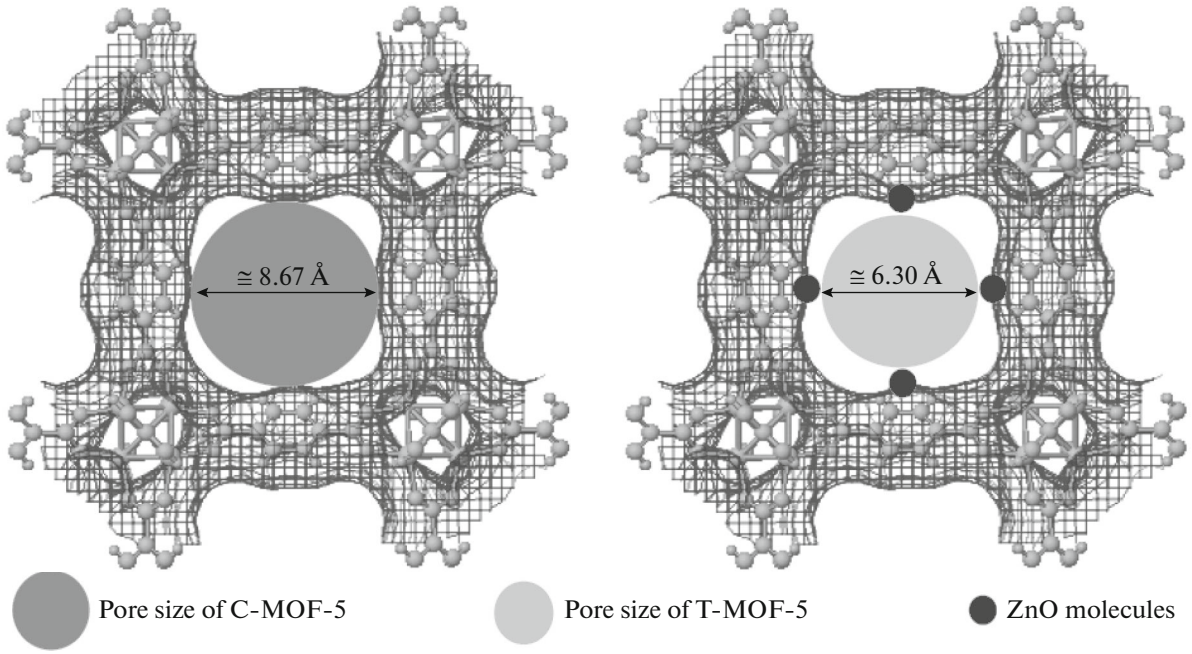

Fig. 1. Schematic pore structure of C-MOF-5 and T-MOF-5.

graphite derivatives, and metal organic frameworks (MOFs), into polymer matrices to form mixed matrix membranes (MMMs) in order to enhance the trade-off limits for separation of various gases [17–31].

Metal-organic frameworks (MOFs), consisting of organic linkers and inorganic joints, have attracted much attention in the past decade due to their potential applications in gas adsorption and storage, drug delivery, and catalysis [32].

As an archetype and representative of MOFs, MOF-5 [structural formula $Zn_4O(BDC)_3$, BDC denotes 1,4-benzenedicarboxylate] received widespread investigations. This framework has potential applications for hydrogen and CO_2 adsorption [33–43].

Skoulidas and Sholl [44] used theoretical techniques and showed that the diffusion of H_2 was much higher than CO_2 and in low pressure, no significant increase of adsorption happened for H_2 and CO_2, while in high pressure, only CO_2 adsorption was increased. Spencer et al. [45] showed that the inorganic cluster of MOF-5 (ZnO) has the primary role for the H_2 adsorption while the organic ligand (BDC) plays only a secondary role. Zhang and Hu [46] reported that there are two types of MOF-5 (Fig. 1): the cubic (C-MOF-5 or activated MOF-5) and tetragonal (T-MOF-5 of non-activated MOF-5) structures, with the composition formulas $Zn_{4.28}O_{12.8}C_{24}H_{11.3}$ and $Zn_4O_{13}C_{24}H_{12.6}(ZnO)_{1.59}(H_2O)_{1.74}$, respectively. The results showed that the composition formula of C-MOF-5 is consistent with the novel MOF-5 ($Zn_4O_{13}C_{24}H_{12}$). Sarmiento-Perez et al. [47] reported a wonderful impact of the BDC organic linker on CO_2 adsorption.

In our previous work [48] we reported that, since T-MOF-5 had more ZnO molecules than the C-MOF-5, the T-MOF-5 had lower porosity, more uniform and smaller pore size and lower surface area than C-MOF-5. The differences between the cubic and tetragonal structure of MOF-5 nanocrystal bring about different behaviours in adsorption and MMMs (as filler) applications. In two other works done by our group [25, 26], we reported synthesis and characterization of C-MOF-5/PEI and T-MOF-5/PEI MMMs to investigate the H_2, CO_2, CH_4 and N_2 permeability, diffusivity and solubility. According to obtained results, the C-MOF-5 and T-MOF-5 show different separation behaviors in MMMs. Finally in a supplementary study, we [43] reported thermogravimetric analysis and adsorption measurements of H_2 and CO_2 on C-MOF-5 and T-MOF- 5 to estimate the amount of increase of ZnO molecules in T-MOF-5 compared to C-MOF-5 and to investigate the effect of more ZnO molecules in T-MOF-5 than those in the C-MOF-5 structure on the gas adsorption properties. According to obtained results, the CO_2 adsorption capacity of C-MOF-5 is more than T-MOF-5 and the H_2 adsorption capacity of C-MOF-5 is less than T-MOF-5 (at 298 K and 25 bar). This behaviour was attributed to more ZnO molecules in T-MOF-5 than C-MOF-5. The results of this study confirm all previous claims [25, 26, 43, 48]. Table 1 summarizes the pore textural property of C-MOF-5 and T-MOF-5 [43].

In this work, we focus on H_2/CO_2 separation using both C-MOF-5 and T-MOF-5 nanocrystals into a cellulose acetate (CA) matrix. Because of its availability, favorable characteristics, excellent hydrolytic resistance, strong membrane structure for durability, compaction-resistant sublayers, wide operating pH and temperature range and ease of manufacturing, CA membrane could be a favored candidate for gas separation (Fig. 2). In order to increase the permeability and improve the selectivity of this polymer, the additive is used in the polymer phase. Also in the selection of polymer materials for fabrication of MMMs, in addition to gas separation properties, the adhesion between polymer and filler must be considered. In fact the C=O and C–OH groups in CA can provide polymer with good compatibility and good affinity to filler for fabrication of MMMs. For these reasons, the CA was chosen as a polymer matrix for fabrication of MMMs containing C-MOF-5 and T-MOF-5. The effects of more ZnO molecules in the structure of T-MOF-5 compared with C-MOF-5 are the purpose of this study. The prepared MOF-5s and MMMs are characterized using powder X-ray diffraction (XRD), fourier-transform infrared spectroscopy (FTIR), scanning electron microscopy (SEM), TGA and single gas permeation.

EXPEIMENTAL

Synthesis of Cubic and Tetragonal MOF-5s

Before synthesis of both MOF-5s, Zinc nitrate hexahydrate ($Zn(NO_3)_2 \cdot 6H_2O$, >99%, Sigma-Aldrich) was stored under nitrogen atmosphere to reduce exposure to moisture.

The C-MOF-5 nanocrystals (activated MOF-5) were synthesized using a method developed by Huang et al. [38]. 0.45 g of $Zn(NO_3)_2 \cdot 6H_2O$ and 0.083 g of Benzene-1,4-dicarboxylic acid (H_2BDC, >99%, Sigma-Aldrich) were dissolved in a mixing of 49 ml of N,N-dimethylformamide (DMF, 99.8%, H_2O < 0.15%, Sigma-Aldrich) and 1 mL of H_2O inside a 100 mL Pyrex media bottle with a Teflon lined lid and then heated to 70°C, under strong agitation. Afterwards, the contents of Pyrex dish were placed in an oven at 100°C for 15 h to obtain large cube-shaped crystals. The reaction vessel was then removed from the oven and allowed to naturally cool down. After filtration, the remained large cube-shaped powder was washed and soaked six times with 60 mL of anhydrous DMF. Then, the DMF was elutriated and the remained powder was washed and soaked six times with 60 ml of anhydrous dichloromethane (CH_2Cl_2, ≥99.8%, Sigma-Aldrich). Finally, the remained activated MOF-5 (C-MOF-5) was dried under vacuum condition at 125°C for 24 h, until white powders were achieved.

Table 1. Pore textural properties of C-MOF-5 and T-MOF-5 nanocrystals [43]

Species	BET specific surface area, m^2/g	Pore diameter, Å	Pore volume, cm^3/g
C-MOF-5	2387	8.67	0.99
T-MOF-5	1280	6.30	0.58

Also the T-MOF-5 nanocrystals (non-activated MOF-5) were synthesized via the approaches developed by Kaye et al. [49]. Accordingly, 1.19 g of $Zn(NO_3)_2 \cdot 6H_2O$ and 0.34 g of H_2BDC were dissolved in a solution containing 40 ml of DMF in a 100 mL Pyrex media bottle with a Teflon lined lid, during stirring at room temperature. Then, three drops of Hydrogen peroxide (H_2O_2, Sigma-Aldrich) were added into reaction vessel. Afterwards, 2.3 mL of triethylamine (TEA, Sigma-Aldrich) was slowly added dropwise into the reaction vessel under strong agitation at 70°C for 2 h. Then the reaction vessel was placed in an oven at 100°C for 15 h. Thereafter the reaction vessel was removed from the oven and allowed to naturally cool down. After elutriation of DMF, the remained powder was washed and filtered with DMF. Finally, the sample (T-MOF-5 or non-activated MOF-5) was dried at 125°C for 24 h under vacuum condition.

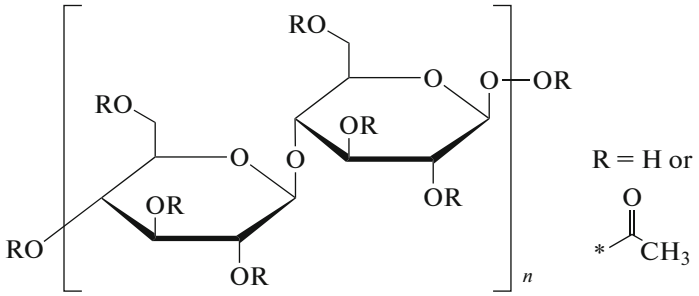

Fig. 2. Structure of CA.

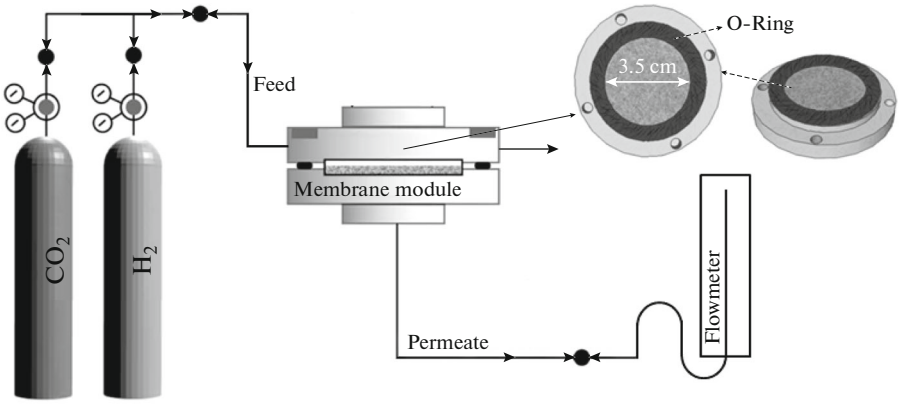

Fig. 3. Schematic of single gas permeation experimental set up.

Fabrication of Pure CA Membrane and MMMs

To obtain the pure CA membrane solution (15 wt %), 0.75 g of the CA (with density of 1.3 g/mL, Sigma-Aldrich) was dissolved in 4.25 g of N-Methyl-2-pyrrolidone (NMP) and stirred for 24 h at 30°C. To fabricate the MOF-5/CA MMMs solution (for both C-MOF-5 and T-MOF-5), the 0.06 g (6% loading), 0.09 g (9%) and 0.12 g (12%) of MOF-5 nanocrystals were added to 3.6 g of NMP and stirred in an ultrasonic water bath for 4 min. Approximately 10% of polymer solution (0.5 g) was then added to the MOF-5s suspension to"prime" the MOF-5s particles. In fact the"priming" technique, which is the adding of low amounts of polymer to the filler suspension before incorporating the particles into the polymer solution to make the particles more compatible with the bulk polymer matrix, promotes greater affinity between the MOF-5s and the CA and usually improves the perm-selectivity properties of the MMMs [21, 50]. The slurry was agitated for 6 h. After good homogenization, the remaining amount of the polymer solution was added to the slurry and the final suspension was agitated again for 1 day. After priming of the MOF-5, 0.84 g (for loading 6%), 0.81 g (9%) and 0.78 g (12%) of CA were added to solution under extreme mobility for 24 h. After placing the pure CA, C-MOF-5/CA and T-MOF-5/CA solutions into three glass vessels overnight, uniform films were casted using a casting knife with thicknesses of 30–40 μm on a glass plate.

The glass plates (containing membranes) were thereafter placed in a vacuum oven at 70°C for 48 h, and the obtained membranes were finally slowly cooled down to ambient temperature in the oven and stored in desiccators before characterization.

Instrumentation and Methods

The XRD, FTIR, SEM, TGA, N_2 adsorption, surface area measurement and pore textural property of both MOF-5s were presented in our previous articles [25, 26, 43, 48]. In this article, SEM images of MMMs were taken using a Cam Scan SEM model KYKYEM3200 microscope. FTIR spectra of the MMMs were recorded at room temperature on a Thermo Nicolet Avatar 370. TGA analyses of MMMs were performed in N_2 atmosphere with TGA-50 Shimadzu.

The pure gas transport properties were measured by the variable-volume/constant-pressure method at 25°C and pressure of 6 bars. The H_2 and CO_2 gas cylinders were obtained from Air Liquid for the permeation experiments. For CO_2, the purity of the gas was greater than 99.5% and for H_2, it was greater than 99.99%. The schema of experimental set-up and membrane module used in this study is shown in Fig. 3.

At steady state condition, gas permeability of species i (P_i) was calculated using the following equation:

$$P_i = \left(\frac{l}{A\Delta P}\right)\left(\frac{dV_i}{dt}\right), \quad (1)$$

$$\alpha_{i,j}^{P} = \frac{P_i}{P_j}, \quad (2)$$

where P_i (P_j) represents the gas permeability of penetrant i (j) (Barrer), ΔP is the transmembrane pressure drop (cm Hg), l is the membrane thickness (cm), A is the effective membrane area (cm^2), dV_i/dt is the permeation rate (cm^3(STP)/s) and $\alpha_{i,j}^{P}$ represents the selectivity of species i over species j (separation factor). The gas permeabilities of prepared membranes were reported in barrer unit, where:

$$P(1\ \text{barrer}) = 10^{-10}\,\frac{\text{cm}^3\,(\text{STP})\text{cm}}{\text{cm}^2\,\text{s}\,\text{cm}\,\text{Hg}}. \quad (3)$$

Or, in SI unit:

$$P(1\ \text{barrer}) = 7.50062\times10^{-18}\,\frac{\text{cm}^3\,(\text{STP})\,\text{m}}{\text{m}^2\,\text{s}\,\text{Pa}}. \quad (4)$$

RESULTS AND DISCUSSION

As mentioned above, all essential analyzes (such as XRD, FTIR, SEM, TGA and N_2 adsorption), surface area measurement and pore textural property of both MOF-5s were presented in our previous works [25, 26, 43, 48]. In the following, the impact of incorporation of C-MOF-5 and T-MOF-5 into CA on the gas separation performance will be investigated.

Membrane Characterization

Morphology by SEM Analysis

Figure 4 shows cross-sections and air-surfaces of the neat CA membrane and the 9 and 12% (*w*/*w*) C-MOF-5/CA and T-MOF-5/CA MMMs. As shown in Figs. 4a, 4f, 4k, the neat CA membrane has a smooth surface and cross-section with a dense structure. According to results of air-surfaces and cross-sections of the MMMs, it is clear that both MOF-5 nanocrystals are well-distributed on the membrane surface (due to ultrasonic homogenization and priming technique) and polymer morphology changes with MOF-5 loading. As shown in Figs. 4k–4o, there are no significant agglomerates or defects to degrade the properties of the MMMs. However, there is a propensity of agglomeration of both MOF-5 particles at high loading. In other word, by increasing the both MOF-5s' content to 12 wt %, some parts of the MOF-5 nanocrystals are agglomerated with each other and some cavities appear inside the MMMs. At high loading, the cavities become more evident in both surface and cross-section. According to results of cross-sections and air-surfaces of the neat CA membrane and MMMs, it can be argued that the C-MOF-5/CA and T-MOF-5/CA contact is acceptable as also is certified by the CO_2 and H_2 permeation results.

FTIR Analysis

The FTIR spectra of the 6, 9 and 12 wt % C-MOF-5/CA and T-MOF-5/CA as well as the spectra of pure CA are shown in Fig. 5. As shown in Fig. 5, all the characteristic peaks of both CA and MOF-5s are present in the MMMs patterns. The neat CA presents bands at 3484 cm^{-1} (OH^- stretching vibrations of the hydroxyl group), 1637 cm^{-1} (interlayer stretching and bending vibration modes of molecular water), 1738 cm^{-1} (C=O stretching), 1368 cm^{-1} (CH_3 symmetric deformation), 1220 cm^{-1} (acetate C–C–O stretching), and 1035 cm^{-1} (C–O stretching) [51, 52]. The peaks around 1590 and 1504 cm^{-1} (two peaks), 1391, 700–1200 and 1010–1250 cm^{-1} (small peaks) are attributed to symmetric stretching of COO groups, asymmetric stretching of COO groups (in carboxylic), terephthalate compounds and C–H group present in the benzene ring of the BDC linker, respectively [38, 53–55]. According to the results, the absorption bands of CA and both MOF-5s were observed in all nanocomposite membranes with slightly shifts in peaks' frequencies. Also the bands at 400–530 cm^{-1} in MOF-5s/CA patterns can be related to stretching of Zn=O [53–56].

Thermal Analysis

The TGA curves of the pure CA and 6, 9 and 12 wt % C-MOF-5/CA and T-MOF-5/CA MMMs are presented in Fig. 6. Three weight loss steps were observed for pure CA: the first step was related to vaporization of water and excess solvent, occurred in the range of 30–260°C; the second step occurred in the range of 260–450°C and was related to the initial thermal decomposition of the polymer chains; and finally, the third step began at about 500°C and was related to the final thermal decomposition of the polymer chains (containing remained carbon). The TGA curves of the MMMs indicate that the weight loss process in MMMs includes more than three steps (containing four steps). This additional step began at about 400°C and was related to decomposition of MOF-5s nanocrystals. Also according to obtained results, it is clear that, addition of both cubic and tetragonal structure of MOF-5, increases thermal resistance of the polymer (CA) matrix. The increase in thermal resistance is attributed to adhesion between MOF-5s and CA matrix and good thermal stability of the MOF-5s. In addition, according to that, C-MOF-5 is more stable than T-MOF-5 [43], and therefore, the C-MOF-5/CA MMMs are more stable than T-MOF-5/CA MMMs.

Gas Permeation

Pure H_2 and CO_2 (see Table 2) permeabilities measurements were performed for neat CA, C-MOF-5/CA and T-MOF-5/CA MMMs. Permeability and ideal selectivity of CA and the all MMMs were summarized in Table 3. In this study, due to the different membrane preparation conditions, the permeability results for pure CA are somewhat different from those previously reported by other research groups [57, 58].

Also the variations in the pure H_2 and CO_2 permeability of the manufactured membranes with respect to C-MOF-5 and T-MOF-5 loading are shown in Fig. 7. According to obtained results, incorporating both C-MOF-5 and T-MOF-5 fillers led to increase in the H_2 permeability, while the CO_2 permeability was initially reduced (in low loading) and then (in high load-

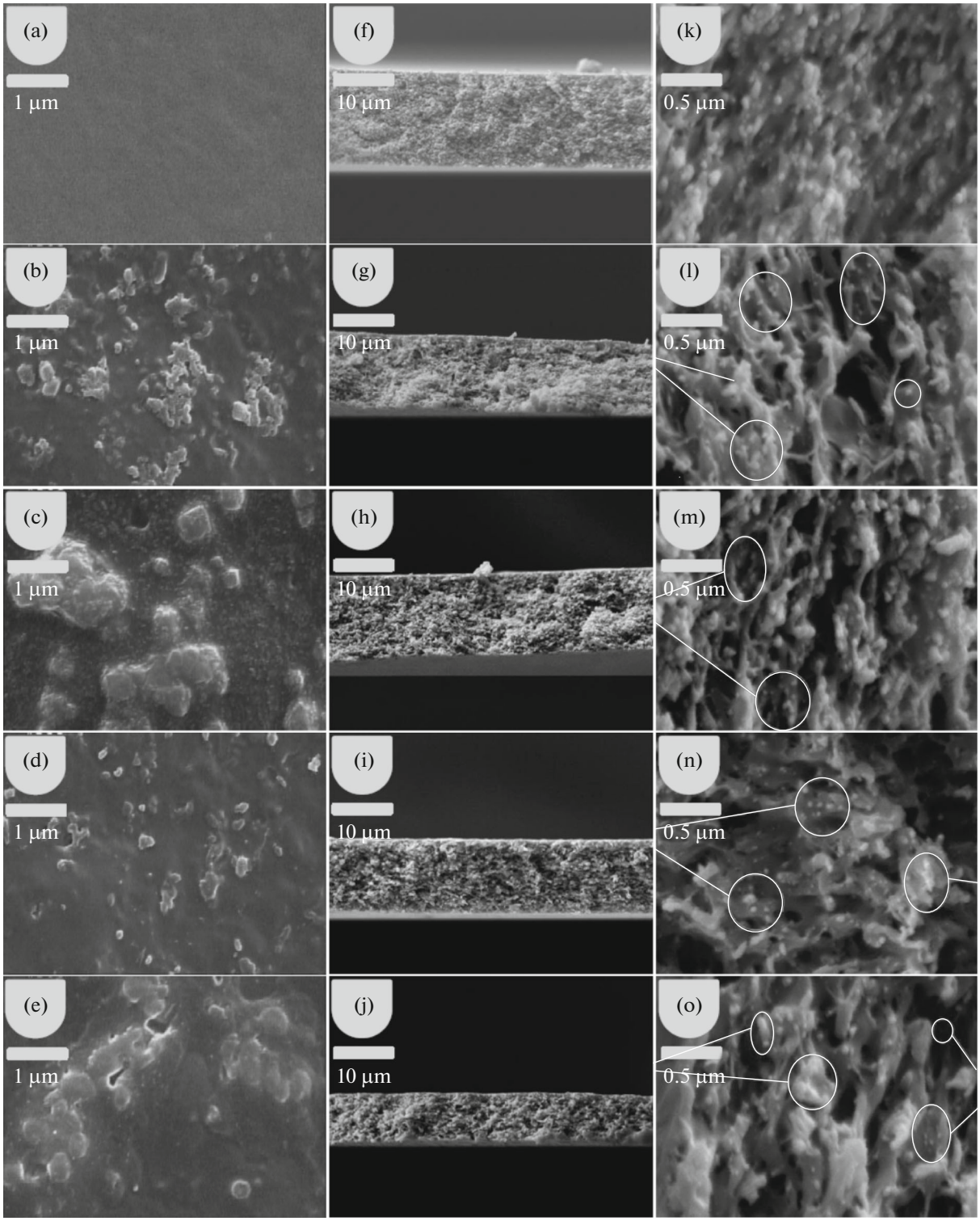

Fig. 4. SEM images of the air-surface (a, b, c, d, and e), cross-section at low magnification (f, g, h, i, and j), and cross-section at high magnification (k, l, m, n, and o) of 0, 9, and 12 wt % C-MOF-5/CA and T-MOF-5/CA MMMs, respectively.

ing) increased. As reported in the previous study [25, 43], for CO_2 gas, the permeability is strongly affected by the solubility and less affected by the diffusion. Also for H_2 gas, relative permeability is more affected by the diffusion than solubility. In other word, the reduction of CO_2 permeability in low loading of both MOF-5s is related to reduction of CO_2 solubility. It is essential to note that, even for CO_2 gas (that its permeability is strongly affected by the solubility), access into the cavities of MOF-5s is a necessary condition. So it is pos-

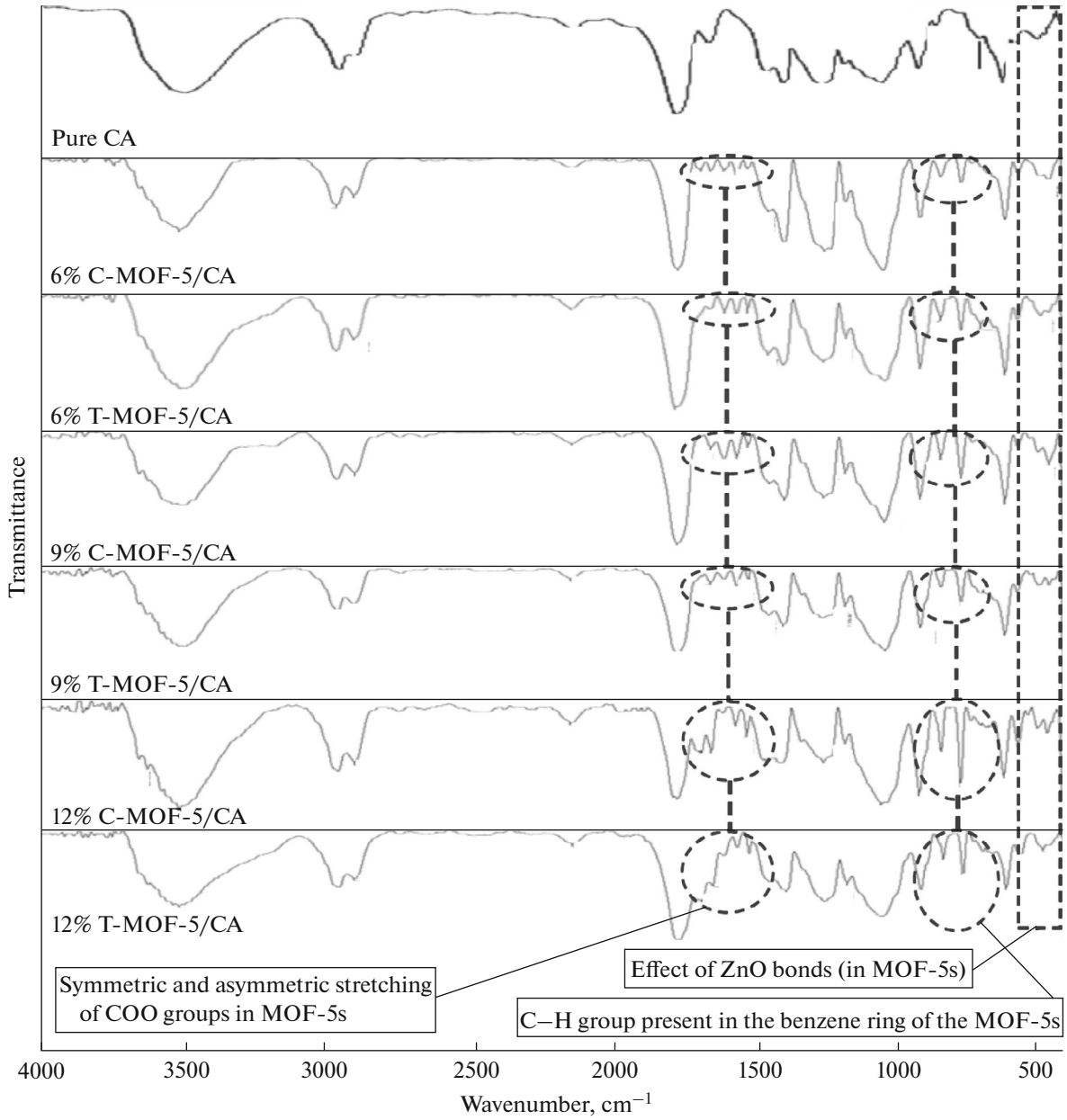

Fig. 5. FTIR spectrums of pure CA, C-MOF-5/CA and T-MOF-5/CA MMMs.

sible that in low loadings of both MOF-5s in CA, a part of pores in MOF-5 can get clogged with polymer chains. This speculation is given credence by H_2 permeability results (low increasing) in low loading of MOF-5s. In other word, since the reducing the size of pores from cubic to tetragonal has little effect on smaller molecule (H_2), it can be expected that the better permeation behavior of H_2 (compared to CO_2) in MMMs (in low loading) is attributed to low diameter of H_2 versus CO_2. As shown in Fig. 7, for both C-MOF-5/CA and T-MOF-5/CA MMMs, the H_2 and CO_2 permeabilities have been substantially increased due to the increase of both C-MOF-5 and T-MOF-5 from 9 to 12%. The mutations in permeability (in high loading) are attributed to increased diffusivity and solubility for H_2 and CO_2, respectively.

The content expressed can be better realized by studying the H_2/CO_2 selectivity coefficient, according to Fig. 8 and Table 3. According to obtained results, for all C-MOF-5 and T-MOF-5 loadings, the H_2/CO_2 selectivity was more than the pure CA membrane. However, with increasing the T-MOF-5 loading from 9 to 12%, the H_2/CO_2 selectivity was decreased as a result of the agglomeration of T-MOF-5 nanocrystals and some cavities appeared within the 12 wt % T-MOF-5/CA MMM. Also for C-MOF-5/CA

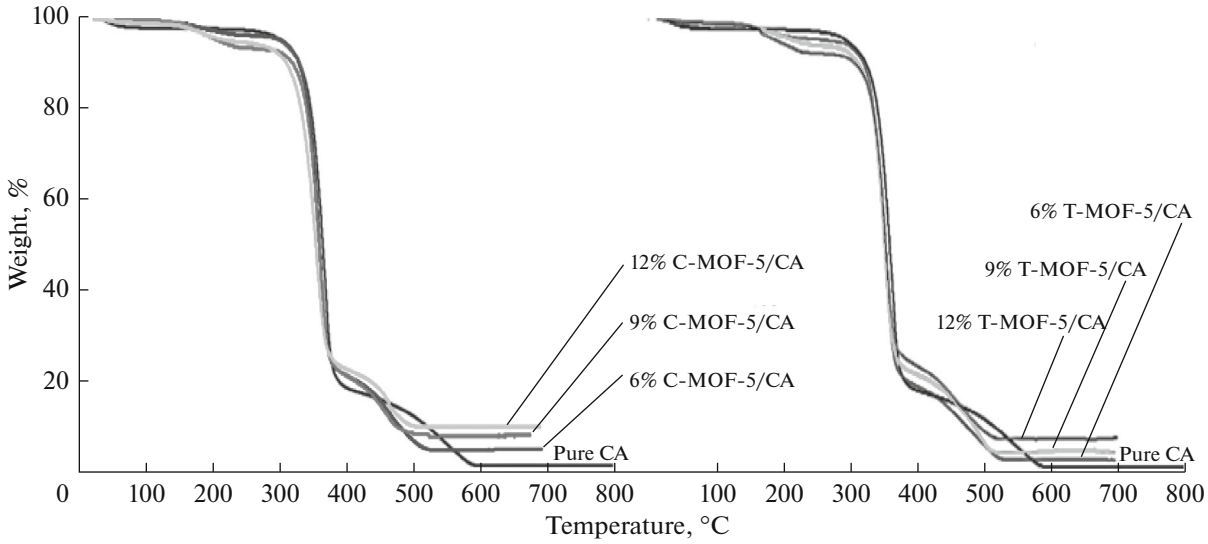

Fig. 6. TGA curves of pure CA and 6, 9, and 12 wt % C-MOF-5/CA and T-MOF-5/CA MMMs.

MMMs, the rate of increase in H_2/CO_2 selectivity for changing the loading from 9 to 12 wt % is lower than that for changing the loading from 6 to 9 wt % (and from neat CA to 6 wt % C-MOF-5/CA MMM). Similar to 12 wt % T-MOF-5/CA MMM, this negative behaviour for 12 wt % C-MOF-5/CA MMM was attributed to some cavities between CA and C-MOF-5 and agglomeration of C-MOF-5 nanocrystals. However for all fabricated MMMs, the H_2/CO_2 selectivity for 12 wt % MOF-5s/CA MMMs is higher than the pure CA membrane and 6 wt % MOF-5s/CA MMMs. The results of H_2/CO_2 selectivity show that the mutations in H_2 and CO_2 permeability (by increasing the loading of MOF-5s from 9 to 12 wt %) are not false and this indicates the availability of the both C-MOF-5 and T-MOF-5 pores.

Although there are many similarities between incorporation of C-MOF-5 and T-MOF-5 nanocrystals into CA matrix, but because the T-MOF-5 has more ZnO molecules in its own_structure [46, 48], the study of differences in transition behavior (permeability and selectivity) for C-MOF-5/CA and T-MOF-5/CA MMMs is very important.

According to Fig. 7a, by changing the filler from C-MOF-5 to T-MOF-5, the appearance of H_2 permeability did not change much, but the CO_2 permeability was reduced. The reasons of these behaviors were attributed to two factors: pore size of both MOF-5 nanocrystals and the presence of more ZnO molecules in T-MOF-5 nanocrystals.

In other word, by changing the filler morphology (from cubic to tetragonal), the pore size of filler was reduced. Because the kinetic diameter of CO_2 is more than H_2, it can be expected that, changing the pore size from C-MOF-5 to T-MOF-5 has more effect on the CO_2 diffusivity. However, by changing the filler from cubic to tetragonal, due to the presence of more ZnO molecules (main adsorption site of H_2) and less BDC molecules (main adsorption site of CO_2) in T-MOF-5 (than C-MOF-5), the adsorption site of H_2 in T-MOF-5 is more than that in C-MOF-5 and also the adsorption site of CO_2 in T-MOF-5 is less than that in C-MOF-5. By changing the filler structure from C-MOF-5 to T-MOF-5, reducing of pore size and also increasing of adsorption site of H_2 (and reduction of adsorption site of CO_2), caused that the appearance of H_2 permeability did not change much but the CO_2 permeability was reduced.

This behavior is well evident in Fig. 8. According to Fig. 8, The H_2/CO_2 selectivity in all T-MOF-5/CA MMMs is higher than all C-MOF-5/CA MMMs.

Furthermore, Table 4 shows a comparison of the results obtained in this study and those of other studies in which MMMs were modified with polymers combined with filler materials. A comparison between the H_2/CO_2 separation performances of our CA/MOF-5 MMMs and literature data shows that our approach is promising (given the about 70% increase in H_2/CO_2 selectivity). Although our CA/MOF-5 MMMs are not quite the best yet, in terms of H_2/CO_2 separation factor

Table 2. Molecular gas properties [44]

Gas	Critical temperature, T_c (K)	Critical volume, V_c, cm^3/mol	Kinetic diameters, Å
H_2	33.20	64.90	2.89
CO_2	304.20	91.90	3.30

Table 3. Gas permeability (barrer) and selectivity of H_2 and CO_2 through the neat CA and MMMs

Samples	H_2	CO_2	H_2/CO_2
Neat CA	4.30 ± 0.52	3.90 ± 0.64	1.10
6 wt % C-MOF-5/CA MMM	4.98 ± 0.50	3.37 ± 0.50	1.48
9 wt % C-MOF-5/CA MMM	6.19 ± 0.40	3.64 ± 0.50	1.70
12 wt % C-MOF-5/CA MMM	14.95 ± 0.70	8.41 ± 0.60	1.78
6 wt %T-MOF-5/CA MMM	4.65 ± 0.40	2.69 ± 0.50	1.73
9 wt % T-MOF-5/CA MMM	6.08 ± 0.60	3.19 ± 0.10	1.91
12 wt % T-MOF-5/CA MMM	13.90 ± 0.70	7.77 ± 0.60	1.79

and permeability, it offers a lot of potential for improvement.

Evaluation of Gas Permeation Performance

A review on the permeability/selectivity data shows an upper bound relationship for polymeric membrane as defined by a Robeson's upper bond trade-off line. The C-MOF-5/CA and T-MOF-5/CA MMMs fabricated in this work reside below or close to the Robeson's upper bond trade-off line for H_2/CO_2 separation (Fig. 9). According to Fig. 9, the incorporation of both C-MOF-5 and T-MOF-5 in neat CA membrane increases the H_2 separation ability of MMMs for H_2/CO_2 separation and this means the fabricated MMMs provide better separation factor than neat CA membrane. As the C-MOF-5 and T-MOF-5 content in CA is increased, the H_2 permeability is increased

Table 4. Comparison of modified polymer by different filler for H_2 and CO_2 separation

Polymer	Filler	wt %	P_{H_2}, barrer	P_{CO_2}, barrer	H_2/CO_2	Ref.
PES	SAPO-34	20	12.6	5.1	2.4	[59]
Matrimid9725	Zeolite 4A	10	28.2	12.8	2.2	[60]
		30	101.6	48.3	2.1	
Matrimid5218	Mesoporous Silica Spheres (MSS)	8	46.9	15	3.1	[61]
PEI	C-MOF-5	25	28.32	5.39	5.25	[25]
Co-polyimide (6FDA-durene)	ZIF-8	15	2136.6	1552.9	1.4	[62]
Co-polyimide (6FDA:DSDA/4MPD:4,4'-SDA)	NH_2 -MIL-101	10	114.0	70.9	1.6	[63]
PPO	Silica	10	548.7	154.1	3.6	[64]
		33.5	103.0	51.0	1.81	[65]
Matrimid@	MIL-53-ht	37.5	66.0	40.0	2.02	
Matrimid@	C-MOF-5	30	53.8	20.2	2.66	[66]
PI	MIL-53(Al)	5	0.416[a]	0.212[a]	1.96	[67]
PI	MOF-5	5	0.239[a]	0.267[a]	0.89	[67]
PI	$Cu_3(BTC)_2$	5	0.437[a]	0.324[a]	1.35	[67]
CA	C-MOF-5	9	6.19	3.64	1.70	This work
		12	14.95	8.41	1.78	
CA	T-MOF-5	9	6.08	3.19	1.91	This work
		12	13.90	7.77	1.79	

[a] GPU.

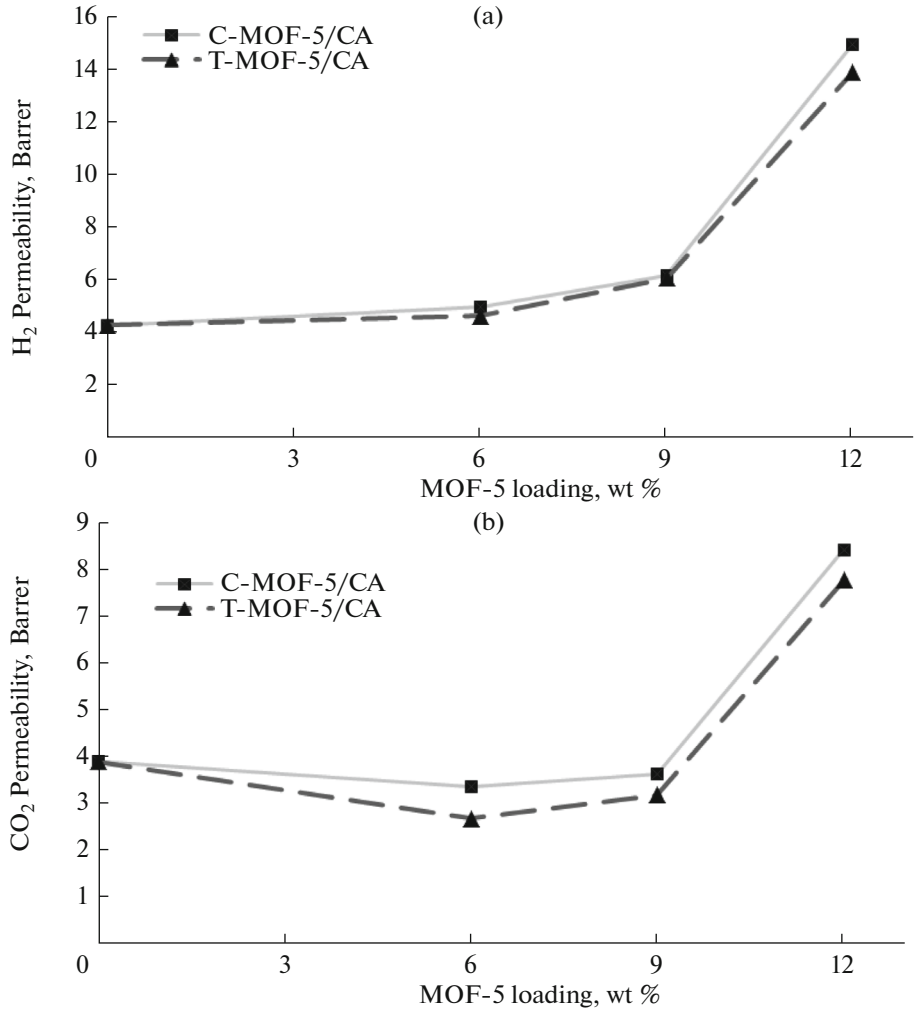

Fig. 7. Plot of permeability versus MOF-5s loading (0, 6, 9, and 12 wt %) for (a) H_2 and (b) CO_2 in both C-MOF-5/CA and T-MOF-5/CA MMMs.

while the selectivity of H_2/CO_2 is slightly increased. Also as shown in Fig. 9, as a result of the more H_2 adsorption site, the T-MOF-5/CA MMMs provide better H_2/CO_2 separation performance than C-MOF-5/CA MMMs.

This research indicated that, the activated MOFs (i.e., C-MOF-5 in this study) are not always the best choices for separation process. In fact this is a qualitative, exploratory study in which the authors are laying the groundwork for future researches on this subject. It is exploratory because no other researches have been conducted on this specific subject.

CONCLUSION

MMMs containing C-MOF-5 and T-MOF-5 nanocrystals and CA polymer were successfully fabricated with excellent adhesion between the both MOF-5s and CA and without sedimentation or agglomeration (at surface) of MOF-5s by controlling of fabrication conditions. The conclusions can be summarized out as follows: (1) according to SEM results of the neat CA membrane and MMMs, it can be argued that the C-MOF-5/CA and T-MOF-5/CA contact is acceptable, (2) addition of both MOF-5s, increases thermal resistance of the CA polymer, (3) the increase in thermal resistance of MMMs is attributed to good adhesion between MOF-5s and CA polymer and good thermal stability of the both MOF-5s, (4) the C-MOF-5/CA MMMs are more stable than T-MOF-5/CA MMMs (because C-MOF-5 is more stable than T-MOF-5), (5) incorporating both MOF-5s in CA leads to increase in the H_2 permeability, while the CO_2 permeability is initially (at 6 wt % of loading) reduced and then (at 9 and 12 wt %) increased, (6) the better permeation behavior of H_2 (compared with CO_2) in MMMs was attributed to lower diameter of H_2, (7) for both C-MOF-5/CA and T-MOF-5/CA MMMs, the H_2 and CO_2 permeabilities have been substantially increased at high load-

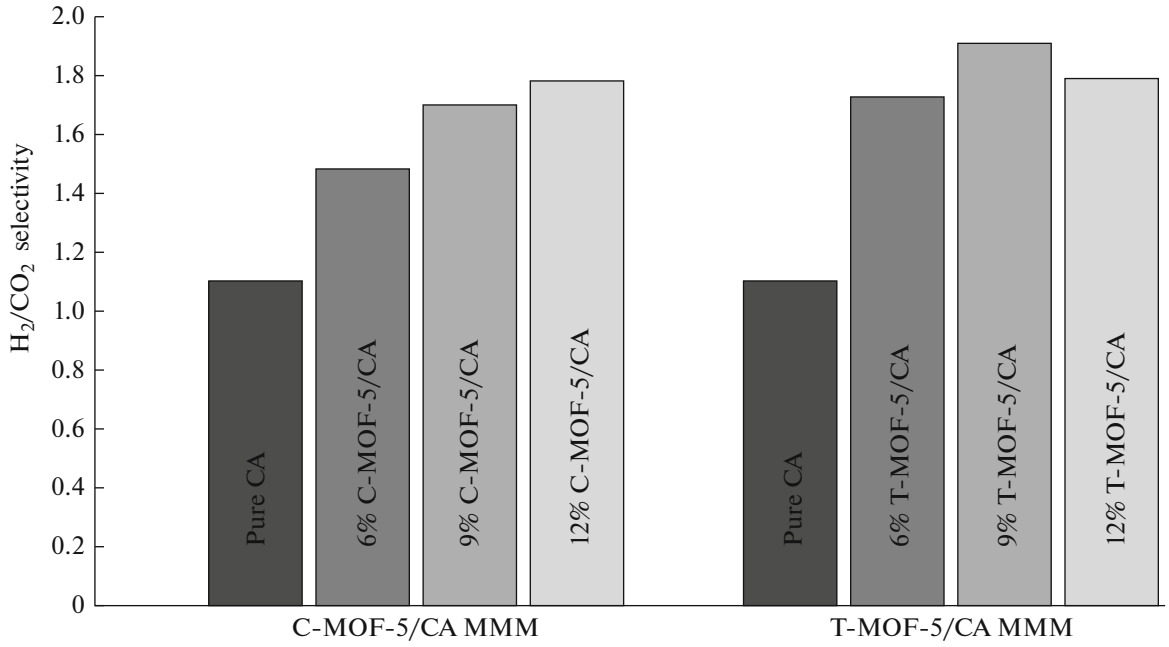

Fig. 8. Ideal selectivity plots of neat CA and 6, 9, and 12 wt % C-MOF-5/CA and T-MOF-5/CA MMMs for H_2/CO_2.

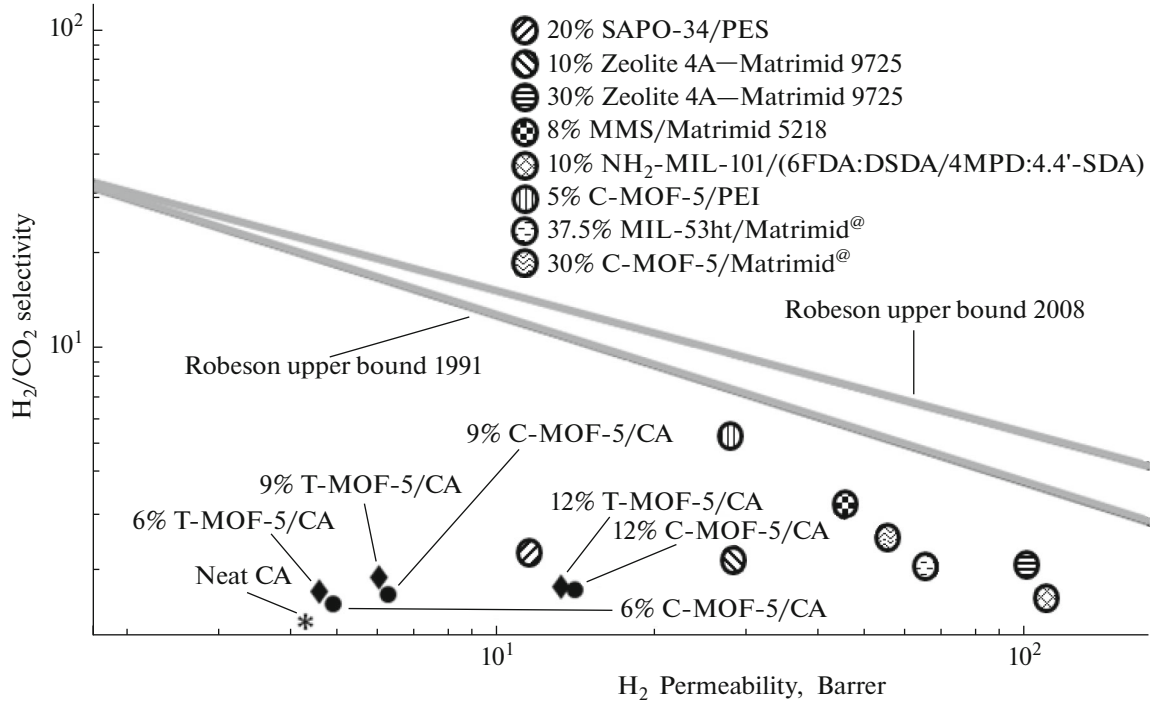

Fig. 9. H_2/CO_2 separation performance of CA, C-MOF-5/CA and T-MOF-5/CA MMMs in comparison to Robeson's upper line.

ing of MOF-5s (these mutations were attributed to increasing of diffusivity and solubility of H_2 and CO_2, respectively), (8) the results of H_2/CO_2 selectivity show that the mutations in H_2 and CO_2 permeability are not false and this demonstrates the availability of the both MOF-5s pores, (9) because of the presence of more ZnO molecules in T-MOF-5, by changing the filler from C-MOF-5 to T-MOF-5, the appearance of H_2 permeability did not change much, but the CO_2 permeability was reduced, (10) the presence of more ZnO molecule in the T-MOF-5 structure could lead to increase the H_2/CO_2.

ACKNOWLEDGMENTS

The authors acknowledge Iran Nanotechnology Initiative Council for financial support.

REFERENCES

1. A. Huang, Y. Chen, Q. Liu, N. Wang, J. Jiang, and J. Caro, J. Memb. Sci. **454**, 126 (2014).
2. R. S. Haszeldine, Science **325**, 1647 (2009).
3. R. W. Baker, Ind. Eng. Chem. Res. **41**, 1393 (2002).
4. N. Z. Muradov and T. N. Veziroglu, Int. J. Hydrogen Energy **33**, 6804 (2008).
5. J. W. Dijkstra, J. A. Z. Pieterse, H. Li, J. Boon, Y. C. Delft, and G. Raju, Energy Procedia **4**, 715 (2011).
6. M. D. Dolan, S. S. Hla, and L. D. Morpeth, Sep. Purif. Technol. **147**, 398 (2015).
7. R. Koc, N. K. Kazantzis, and M. Y. Hua, Int. J. Hydrogen Energy **36**, 4934 (2011).
8. T. A. Peters, M. Stange, H. Klette, and R. Bredesen, J. Membr. Sci. **316**, 119 (2008).
9. E. Fernandez, K. Coenen, A. Helmi, J. Melendez, J. Zuñiga, and D. A. Pacheco Tanaka, Int. J. Hydrogen Energy **40**, 13463 (2015).
10. H. B. Wang and Y. S. Lin, J. Membr. Sci. **396**, 128 (2012).
11. S. Smart, J. Vente, J. and C. Diniz da Costa, Int. J. Hydrogen Energy **37**, 12700 (2012).
12. A. Criscuoli, A. Basile, and E. Drioli, Catal. Today **56**, 53 (2000).
13. C. A. Scholes, K. H. Smith, S. E. Kentish, and G. W. Stevens, Int. J. Greenhouse Gas Control **4**, 739 (2010).
14. D. R. Pesiri, B. Jorgensen, and R. C. Dye, J. Membr. Sci. **218**, 11 (2003).
15. E. V. Perez, K. J. Balkus, J. P. Ferraris, and I. H. Musselman, J. Membr. Sci. **328**, 165 (2009).
16. H. B. Tanh Jeazet, C. Staudt, and Ch. Janiak, Dalton Trans. **41**, 14003 (2012).
17. W. J. Koros and R. Mahajan, J. Membr. Sci. **175**, 181 (2000).
18. W. J. Koros and R. Mahajan, Polym. Eng. Sci. **42**, 1420 (2002a).
19. W. J. Koros and R. Mahajan, Polym. Eng. Sci. **42**, 1432 (2002b).
20. J.-M. Duval, B. Folkers, M. H. V. Mulder, G. Desgrandchamps, and C. A. Smolders, J. Membr. Sci. **80**, 189 (1993).
21. R. Mahajan and W. J. Koros, Ind. Eng. Chem. Res. **39**, 2692 (2000).
22. M. G. Suer, N. Bac, and L. Yilmaz, J. Membr. Sci. **91**, 77 (1994).
23. M. Pakizeh and S. Hokmabadi, J. Appl. Polym. Sci. **134**, 443291 (2016).
24. A. Ehsani and M. Pakizeh, J. Taiwan Inst. Chem. Eng. **66**, 414 (2016).
25. M. Arjmandi and M. Pakizeh, J. Ind. Eng. Chem. **20**, 3857 (2014).
26. M. Arjmandi, M. Pakizeh, and O. Pirouzram, Korean J. Chem. Eng. **32**, 1178 (2015).
27. H. Amedi and M. Aghajani, J. Nat. Gas Sci. Eng. **35**, 695 (2016).
28. E. Ahmadpour, M. V. Sarfaraz, R. Mosayyebi Behbahani, A. Arabi Shamsabadi, and M. Aghajani, J. Nat. Gas Sci. Eng. **35**, 33 (2016).
29. A. Jomekiana, R. Mosayebi Behbahani, T. Mohammadi, and A. Kargari, J. Nat. Gas Sci. Eng. **31**, 562 (2016).
30. F. Dorosti, M. Omidkhah, and R. Abedini, J. Nat. Gas Sci. Eng. **25**, 88 (2015).
31. M. Farrokhnia, A. Safekordi, M. Rashidzadeh, G. Khanbabaei, R. Akbari Anari, and M. Rahimpour, J. Porous Mater. **23**, 1279 (2016).
32. O. Ghaffari Nik, X. Y. Chen, and S. Kaliaguine, J. Membr. Sci. **413–414**, 48 (2012).
33. H. Li, M. Eddaoudi, M. O'Keeffe, and O. M. Yaghi, Nature **402**, 276 (1999).
34. M. Dinca, A. Dailly, Y. Liu, C. M. Brown, D. A. Neumann, and J. R. Long, J. Am. Chem. Soc. **128**, 16876 (2006).
35. N. L. Rosi, J. Eckert, M. Eddaoudi, D. T. Vodak, J. Kim, M. O'Keeffe, and O. M. Yaghi, Science **300**, 1127 (2003).
36. M. Müller, S. Hermes, K. Kähler, M. W. E. van den Berg, M. Muhler, and R. A. Fischer, Chem. Mater. **20**, 4576 (2008).
37. F. Salles, H. Jobic, G. Maurin, M. M. Koza, P. L. Llewwellyn, T. Devic, C. Serre, and G. Ferey, Phys. Rev. Lett. **100**, 245901 (2008).
38. L. Huang, H. Wang, J. Chen, Z. Wang, J. Sun, D. Zhao, and Y. Yan, Microporous Mesoporous Mater. **58**, 105 (2003).
39. R. E. Morris and P. S. Wheatley, Angew. Chem. Int. Ed. **47**, 4966 (2008).
40. J. Y. Lee, L. Pan, S. R. Kelly, J. Jagiello, T. J. Emge, and J. Li, Adv. Mater. **17**, 2703 (2005).
41. M. Hirscher and B. Panella, Scr. Mater. **56**, 809 (2007).
42. J. S. Choi, W. J. Son, J. Kim, and W. S. Ahn, Microporous Mesoporous Mater. **116**, 727 (2008).
43. M. Arjmandi and M. Pakizeh, Braz. J. Chem. Eng. **33**, 225 (2015).
44. A. I. Skoulidas and D. S. Sholl, J. Phys. Chem. B **109**, 15760 (2005).

45. E. C. Spencer, J. A. K. Howard, G. J. McIntyre, J. L. C. Rowsell, and O. M. Yaghi, Chem. Commun. (Cambridge, U. K.) **21**, 278 (2006).
46. L. Zhang and Y. H. Hu, Mater. Sci. Eng., B **176**, 573 (2011).
47. R. A. Sarmiento-Perez, L. M. Rodriguez-Albelo, A. Gomez, M. Autie-Perez, D. W. Lewis, and A. R. Ruiz-Salvador, Micoporous Mesoporous Mater. **163**, 186 (2012).
48. M. Arjmandi and M. Pakizeh, Acta Metall. Sin. (Engl. Lett.) **26**, 597 (2013).
49. S. S. Kaye, A. Dailly, O. M. Yaghi, and J. R. Long, J. Am. Chem. Soc. **129**, 14176 (2007).
50. G. Clarizia, C. Algieri, A. Regina, and E. Drioli, Microporous Mesoporous Mater. **115**, 67 (2008).
51. Y. Yang, in *Polymer Data Handbook*, Ed. by J. E. Mark (Oxford Univ. Press, New York, 1999).
52. N. Benosmane, B. Guedioura, S. M. Hamdi, M. Hamdi, and B. Boutemeur, Mater. Sci. Eng., C **30**, 860 (2010).
53. S. Hermes, F. Schroder, S. Amirjalayer, R. Schmid, and R. A. Fischer, J. Mater. Chem. **16**, 2464 (2006).
54. R. Sabouni, H. Kazemian, and S. Rohani, Chem. Eng. J. **165**, 966 (2010).
55. N. T. S. Phan, K. K. A. Le, and T. D. Phan, Appl. Catal., A **382**, 246 (2010).
56. J. Coates, (Wiley, New York, 2000).
57. V. Abetz, T. Brinkmann, M. Dijkstra, K. Ebert, D. Fritsch, K. Ohlrogge, D. Paul, K.-V. Peinemann, S. P. Nunes, N. Scharnagk, and M. Schossig, Adv. Eng. Mater. **8**, 328 (2006).
58. R. W. Baker, *Membrane Technology and Application*, 2nd ed. (Wiley, California, 2004).
59. E. Karatay, H. Kalıpcılar, and L. Yılmaz, J. Membr. Sci. **364**, 75 (2010).
60. J. Ahmad and M. B. Hagg, Sep. Purif. Technol. **115**, 190 (2013).
61. B. Zornoza, O. Esekhile, W. J. Koros, C. Tellez, and J. Coronas, Sep. Purif. Technol. **77**, 137 (2011).
62. B. Seoane, C. Tellez, J. Coronas, and C. Staudt, Sep. Purif. Technol. **111**, 72 (2013).
63. S. N. Wijenayake, N. P. Panapitiya, S. H. Versteeg, C. N. Nguyen, S. Goel, and K. J. Balkus, Ind. Eng. Chem. Res. **52**, 6991 (2013).
64. G. L. Zhuang, H. H. Tseng, and M. Y. Wey, Int. J. Hydrogen Energy **39**, 17178 (2014).
65. J. O. Hsieh, K. J. Balkus, J. P. Ferraris, and I. H. Musselman, Microporous Mesoporous Mater. **196**, 165 (2014).
66. E. V. Perez, K. J. Balkus, J. P. Ferraris, and I. H. Musselman, J. Membr. Sci. **328**, 165 (2009).
67. H. Ren, J. Jin, J. Hu, and H. Liu, Ind. Eng. Chem. Res. **51**, 10156 (2012).